

# ISR Hadron Production in $e^+e^-$ Annihilations and Meson-Photon Transition Form Factors

D. R. Muller  
SLAC National Accelerator Laboratory, Stanford, CA, USA and  
Representing the BaBar collaboration

We present several recent results from the BaBar collaboration in the areas of initial state radiation physics and transition form factors. An updated study of the processes  $e^+e^- \rightarrow K^+K^-\pi^+\pi^-$  and  $e^+e^- \rightarrow K^+K^-\pi^0\pi^0$  provides an improved understanding of the  $Y(2175)$  meson. A very precise study of the process  $e^+e^- \rightarrow \pi^+\pi^-$  improves the precision on the calculated anomalous magnetic moment of the muon and provides by far the best information on excited  $\rho$  states. Our previous measurements of the timelike transition form factors (TFF) of the  $\eta$  and  $\eta'$  mesons at  $Q^2 = 112 \text{ GeV}^2$ , combined with new measurements of the their spacelike TFFs and those of the  $\pi^0$  and  $\eta_c$  mesons, provide powerful tests of QCD and models of the distribution amplitudes of quarks inside these mesons. The  $\eta_c$  TFF shows the expected behavior over the  $Q^2$  range 1–50  $\text{GeV}^2$ , and we are sensitive to next-to-leading-order QCD corrections. The  $\eta$  and  $\eta'$  TFFs are consistent with expected behavior, but those for the  $\pi^0$  are not. Extracting the strange and nonstrange components of the  $\eta$  and  $\eta'$  TFFs, we find the nonstrange component to be consistent with theoretical expectations and inconsistent with the measured  $\pi^0$  TFF.

## 1. Introduction

The BaBar experiment studies electron-positron annihilations at a center-of-mass (CM) energy  $\sqrt{s}=10.6 \text{ GeV}$ . It features a boosted CM system and a state of the art, asymmetric detector, which were designed for the study of CP violation in the  $B$  meson system at the very high luminosity PEP-II  $B$  factory. These features also enable a wide range of additional physics at and below the nominal  $\sqrt{s}$ . Here we consider recent results in two such areas: initial state radiation (ISR), which gives access to  $e^+e^-$  annihilations at lower CM energies; and two-photon collisions, which can produce final states with quantum numbers such as  $J^{PC} = 0^{-+}$  that are inaccessible via annihilations.

## 2. Initial State Radiation

An incoming electron or positron can radiate an energetic photon before annihilating with an oncoming positron or electron, respectively, at a reduced CM energy  $\sqrt{s'}=\sqrt{s}-E_\gamma$  where  $E_\gamma$  is the energy of the radiated photon. This process is well understood theoretically, so that cross sections for and characteristics of particular types of events can be measured over a wide range of  $\sqrt{s'}$  in a single experiment. If the ISR photon is well within the detector acceptance, as it is about 12% of the time in BaBar, then the hadronic system is also well contained, with full acceptance in all kinematic variables. Furthermore, the hadronic system is boosted, allowing good measurements of kinematic quantities for energies all the way down to threshold. However, the ISR cross section is low, so that high luminosity is required to make meaningful measurements.

In BaBar, we have studied a large number of exclusive hadronic final states produced via ISR. In each case, we select events with a high-energy photon candidate recoiling against a particular number of charged tracks and additional photons, identify the tracks as pions, kaons or protons, and combine photons to form  $\pi^0$  candidates. We then subject the set of reconstructed particles to a number of kinematic fits that impose 4-momentum conservation under various hypotheses for the event type. We select events with a good  $\chi^2$  for the signal hypothesis and poor  $\chi^2$  for certain alternative hypotheses, evaluate remaining backgrounds from the data and subtract them. We derive cross sections as functions of  $\sqrt{s'}$  using efficiencies derived from the data, and study the structure of the events, in particular any resonant contributions. Here we present updated results on the  $K^+K^-\pi^+\pi^-$  and  $K^+K^-\pi^0\pi^0$  final states, and new results on the  $\pi^+\pi^-$  final state.

### 2.1. The $e^+e^- \rightarrow K^+K^-\pi^+\pi^-$ and $e^+e^- \rightarrow K^+K^-\pi^0\pi^0$ Processes

We have updated our earlier study [1] of the final states comprising two charged kaons and either two charged or two neutral pions using a larger data sample [2]. The largest backgrounds are from other ISR processes with similar kinematics, namely  $K_S^0 K^\pm \pi^\mp$ ,  $\pi^+\pi^-\pi^+\pi^-$ ,  $\pi^+\pi^-\pi^0\pi^0$ ,  $K^+K^-\pi^0$ ,  $K^+K^-\eta$  and  $K^+K^-\pi^0\pi^0\pi^0$ , all of which we have measured previously. The backgrounds from  $e^+e^- \rightarrow q\bar{q} \rightarrow \pi^0 K^+K^-\pi\pi$ , where an isolated,

energetic  $\pi^0$  mimics an ISR photon, are also substantial. We measure them in the data by combining the ISR photon with additional energy clusters in the event and fitting the  $\pi^0$  peaks in the resulting invariant mass distributions. These backgrounds are at the few percent level at low  $\sqrt{s'}$ , but become relatively large at higher energies, limiting the range of our measurements to about 5 GeV.

We calibrate the efficiencies for particle reconstruction and identification from the data, and use them to convert the observed numbers of events in each  $\sqrt{s'}$  bin into the cross sections shown in Fig. 1. These supersede our previous measurements. The  $K^+K^-\pi^+\pi^-$  measurement is consistent with and far more precise than the only other measurement, from the DM1 collaboration [3], for energies below 2.2 GeV. Ours remains the only measurement at higher energies, extending to 5 GeV, and our measurement of the  $K^+K^-\pi^0\pi^0$  cross section from threshold to 4 GeV is also still unique. The errors shown are statistical; there is an overall 5% (7%) systematic uncertainty on the  $K^+K^-\pi^+\pi^-$  ( $K^+K^-\pi^0\pi^0$ ) cross section.

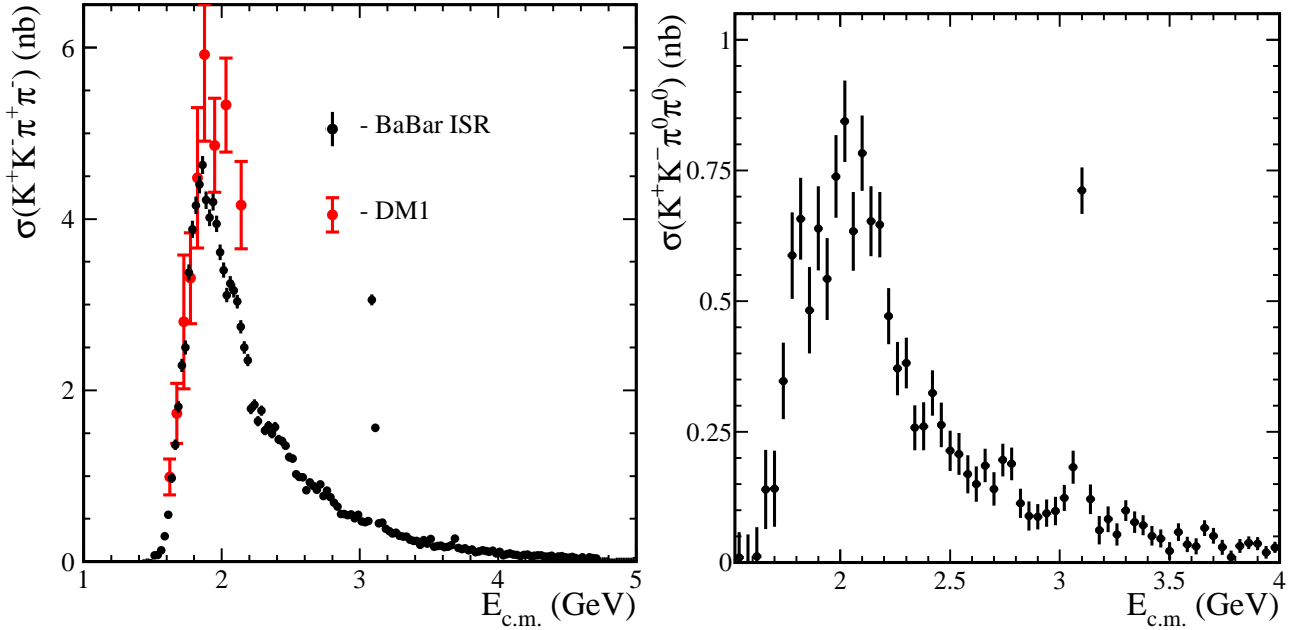


Figure 1: Cross sections for the processes  $e^+e^- \rightarrow K^+K^-\pi^+\pi^-$  (left) and  $e^+e^- \rightarrow K^+K^-\pi^0\pi^0$  (right) as functions of the  $e^+e^-$  CM energy  $E_{c.m.} = \sqrt{s'}$ . Previous results from the DM1 experiment are also shown, in red.

Both cross sections are very small from threshold up to about 1.6 GeV, at which point they rise quickly to peak values of about 5 nb and 0.8 nb, and then fall with increasing  $\sqrt{s'}$ . A narrow  $J/\psi$  peak is clear in both final states, and a  $\psi(2S)$  peak is visible in the  $K^+K^-\pi^+\pi^-$  mode. The  $K^+K^-\pi^+\pi^-$  cross section also shows considerable structure in the 1.8–3 GeV region, and similar features may be present in the  $K^+K^-\pi^0\pi^0$  cross section, though they cannot be resolved with the current statistics.

Both final states are dominated by the quasi-3-body submodes  $K^*(890)K\pi$ ,  $K^*(1430)K\pi$ ,  $K^+K^-\rho$  and  $\phi\pi\pi$ . There are substantial contributions from the quasi-2-body modes  $K^*(890)\bar{K}^*(890)$ ,  $K^*(890)\bar{K}^*(1430)$ ,  $K_1^+(1270)K^-$  and  $\phi f_0(980)$ . We derive cross sections for most of these modes individually by fitting sets of invariant mass distributions. The  $\phi\pi\pi$  and  $\phi f_0(980)$  contributions are particularly interesting, and their cross sections are shown in Fig. 2. The peaks near threshold in the  $\phi\pi\pi$  cross sections (left and middle plots) are expected from the  $\phi(1680)$  resonance. The peaks at higher masses are from the  $Y(2175)$ , a state first reported by us [1], since confirmed by the BES [4] and Belle (as shown in Fig. 2) [5] experiments, and seen in this study with a significance exceeding nine standard deviations.

These cross sections can be described using only two contributions, a  $\phi(1680)$  that decays into both  $\phi\pi\pi$  and  $\phi f_0$ , and a  $Y(2175)$  that decays only into  $\phi f_0$ . A combined fit to these and other cross sections yields improved measurements of the mass and width of the  $Y(2175)$ , as well as its production cross section and phase with respect to the  $\phi(1680)$ :

$$\begin{aligned} m_Y &= 2180 \pm 8 \pm 8 \text{ MeV}/c^2; \\ \Gamma_Y &= 77 \pm 15 \pm 15 \text{ MeV}; \\ \sigma_Y &= 93 \pm 21 \pm 10 \text{ pb}; \\ \psi_Y &= -2.11 \pm 0.24 \pm 0.12 \text{ rad.} \end{aligned}$$

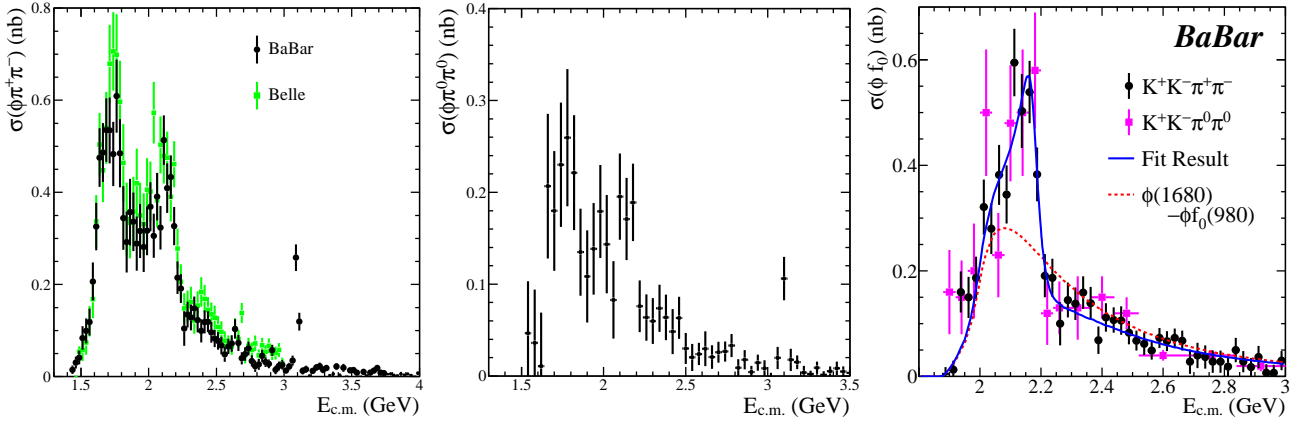


Figure 2: Cross sections for the processes  $e^+e^- \rightarrow \phi\pi^+\pi^-$  (left) and  $e^+e^- \rightarrow \phi\pi^0\pi^0$  (middle) vs.  $\sqrt{s'}$ . The right plot shows the cross sections for  $e^+e^- \rightarrow \phi f_0$  measured in the  $K^+K^-\pi^+\pi^-$  (black) and  $K^+K^-\pi^0\pi^0$  (magenta) final states. The blue line is the result of the fit described in the text, with the dashed red line indicating the  $\phi(1680)$  component.

The result of the fit is shown as the blue line on the right-hand plot in Fig. 2. Here, the  $\phi f_0$  cross sections measured in the two final states are overlaid and seen to be consistent. The contribution from the  $\phi(1680)$ , shown in red, is well constrained by the  $\phi\pi\pi$  cross sections, and the sharp drop near 2.2 GeV is well described by destructive interference between the two resonances.

The interpretation of this state remains unclear. It is unlikely to be an excited  $\phi$  state, since we observe no signal when the  $\pi^+\pi^-$  pair is outside the  $f_0$  region. It could be a strangeonium-like state analogous to one of the many recently discovered charmonium-like states.

## 2.2. The $e^+e^- \rightarrow \pi^+\pi^-$ Process

Recently, we have completed a precise measurement of the final state comprising only two charged pions [6]. Here we aim for precision better than 1%, so the analysis is more detailed. The largest backgrounds are from ISR  $\mu^+\mu^-$  and ISR  $K^+K^-$  production, and we measure these two processes simultaneously with the signal. Since there are  $\sqrt{s'}$  regions in which each of these dominates, we are able to calibrate all particle identification and misidentification rates reliably from the data. We measure the backgrounds from  $e^+e^- \rightarrow q\bar{q} \rightarrow \pi^0\pi^+\pi^-$  and  $\pi^0 K^+K^-$  from the data, as described above, and take those from other ISR processes from our previous measurements. The latter backgrounds are very low below about 1.4 GeV, but become important rapidly at higher  $\sqrt{s'}$ .

We measure track finding efficiencies separately for muons, pions, and kaons, as well as the correlated efficiency for the two tracks in a pair, which is driven by their proximity halfway through the tracking volume. Similarly, we measure track identification efficiencies and their correlations in the data, with the correlations driven by dead and inefficient regions of the muon and hadron identification systems. We also measure the trigger efficiencies using redundant triggers.

The effects of higher order initial and final state radiation (FSR) are important. We study these by considering each additional energy cluster in each selected event as an FSR candidate and performing a kinematic fit under this hypothesis. We also consider the hypothesis of an additional ISR photon emitted along the beam line and not detected. From the distributions of the changes in  $\chi^2$  for these various additions, we measure the product of higher order effects and our acceptance for such events, which we find to be consistent with our simulation. This study also gives additional constraints on several of the important backgrounds.

After verifying that our measured  $\mu$ -pair cross section agrees with the predictions of QED within our overall uncertainty of better than 1.7% (see Fig. 3), we derive our  $\pi^+\pi^-$  cross section from the ratio of our  $\pi^+\pi^-$  and  $\mu^+\mu^-$  measurements and QED. This cancels or reduces several of the systematic uncertainties. The resulting cross section is shown in Fig. 3 and covers by far the widest range of any single experiment, from threshold to 3 GeV. In the regions below 0.6 GeV and between 1 and 1.4 GeV, our systematic uncertainty is about 0.8% and we are consistent and competitive with previous results. We have the world-best results in the regions 0.3–0.4 and 1.4–2.2 GeV, and the only measurement above 2.2 GeV. We observe considerable structure above 1.2 GeV that requires at least three excited  $\rho$  states for a good description. This measurement will increase the understanding of such states dramatically.

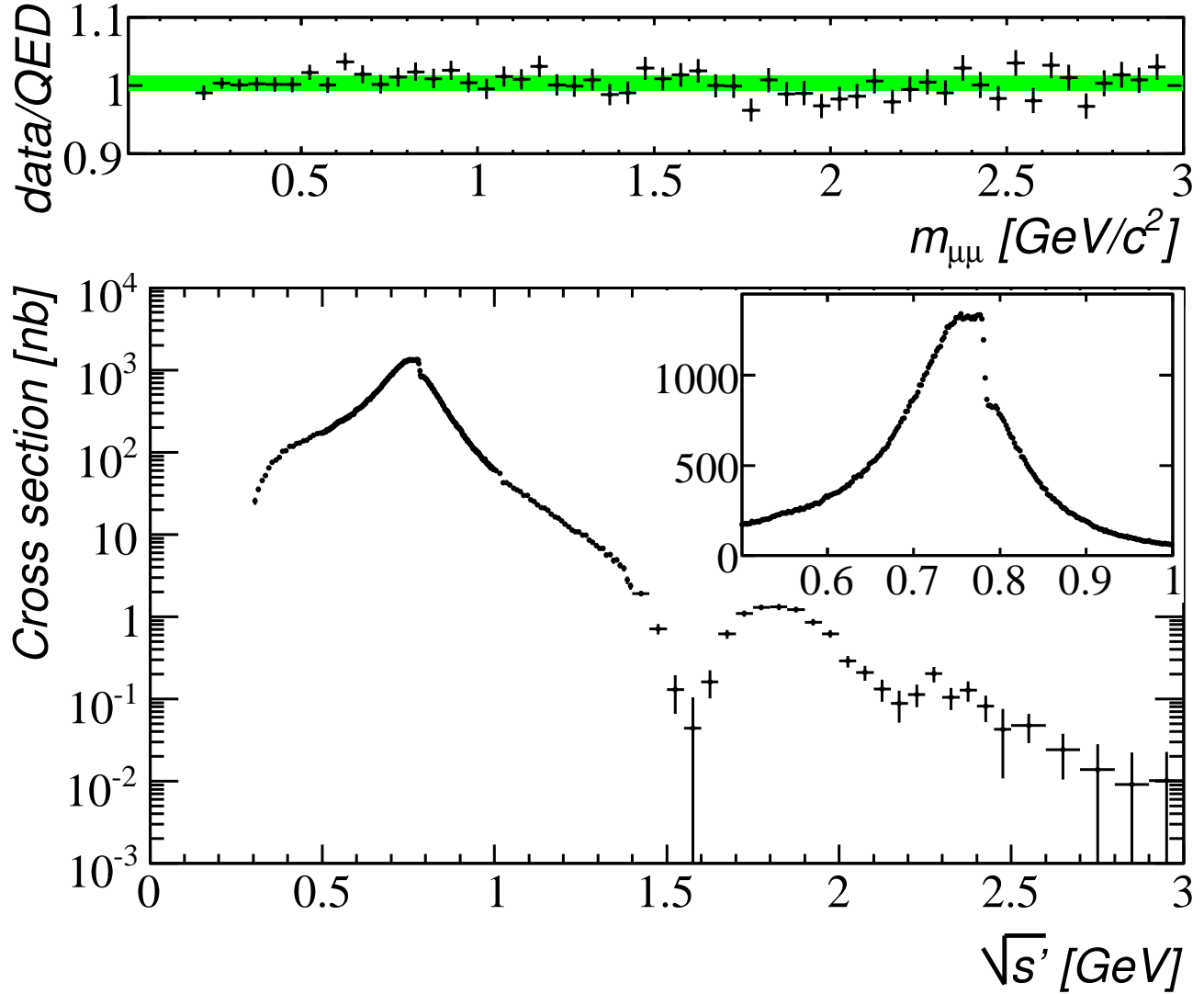


Figure 3: Top: ratio of the measured  $\mu$ -pair cross section to the prediction of QED. The data points are shown with statistical errors and the green band represents the systematic uncertainty. Bottom: the cross section for the process  $e^+e^- \rightarrow \pi^+\pi^-$  as a function of  $e^+e^-$  CM energy.

The cross section shows a very large peak due to the  $\rho(770)$ , and its interference with the  $\omega$  is clearly visible, with detail shown in the inset. In this region, our systematic uncertainty is 0.5%, slightly better than the 0.8% on the next best results, from the CMD-2 [7] and KLOE [8] experiments. There is also a 1.5% measurement from the SND experiment [9]. Results from all experiments are consistent, but they do show variations in both the overall normalizations and slopes at the level of the systematic uncertainties. As with many high precision measurements, the interpretation can be rather sensitive to small changes in such variables, and it is very important to have multiple independent measurements with similar precision,

In particular, there is a long standing discrepancy between the experimentally measured value of the anomalous magnetic moment of the muon,  $a_\mu = g_\mu - 2$  and its theoretical calculation. The calculation of the hadronic loop contribution  $a_\mu^{\text{had}}$  requires the total  $e^+e^- \rightarrow \text{hadrons}$  cross section as input to a convolution integral. The kernel is proportional to  $1/s$ , so that the low-energy cross section dominates the integral, and that is exclusively (predominantly) from the  $\pi^+\pi^-$  final state below 0.6 (1.0) GeV.

We have also measured most of the final states that contribute in the 1–3 GeV region. Taken together, our measurements have improved the uncertainty on  $a_\mu^{\text{had}}$  by about 20%, with about half the improvement from this measurement of the  $\pi^+\pi^-$  final state. A current global fit [10] gives a value of  $a_\mu$  that differs from the experimental value by  $29 \pm 8 \times 10^{-10}$ , or 3.6 standard deviations. These measurements will have a similar effect on the calculation of the running fine structure constant  $\alpha(M_Z)$ .

### 3. Transition Form Factors

A transition form factor (TFF)  $F_X(q_1^2, q_2^2)$  characterizes the coupling of a meson  $X$  to a pair of (virtual) photons with squared invariant masses  $q_1^2$  and  $q_2^2$ . Its dependence on the  $q_i^2$  can be related to the distribution amplitudes of quarks within the meson  $X$ , providing a test of models for such amplitudes. Its asymptotic value when one photon is real and the other highly virtual can be related to meson's decay constant,  $f_X$ , providing a test of QCD.

#### 3.1. Timelike TFFs

We have measured the cross sections for the processes  $e^+e^- \rightarrow \gamma^* \rightarrow \eta\gamma$  and  $e^+e^- \rightarrow \gamma^* \rightarrow \eta'\gamma$  [11]. In each case, there is a real photon in the final state, i.e.  $q_2^2 = 0$ , and a virtual photon with  $Q^2 = q_1^2 = 10.6^2 \text{ GeV}^2$  in the propagator, so that these cross sections can be related to the TFFs  $F_\eta(Q^2)$  and  $F_{\eta'}(Q^2)$ . The TFF is denoted timelike since  $Q^2$  is positive, and the second argument is dropped when  $q_2^2 = 0$ .

As in our ISR analyses, we select events with an energetic photon recoiling against either a  $\pi^+\pi^-\pi^0$  system or a  $\pi^+\pi^-\eta$  system in which the  $\eta$  candidate is formed from a  $\gamma\gamma$  pair or a  $\pi^+\pi^-\pi^0$  combination. A set of kinematic fits combined with selection criteria optimized for this process yields very clean samples of  $e^+e^- \rightarrow \pi^+\pi^-\pi^0\gamma$  and  $e^+e^- \rightarrow \pi^+\pi^-\eta\gamma$  events. Since pseudoscalar mesons cannot be produced exclusively via  $e^+e^-$  annihilation, a peak in the  $\pi^+\pi^-\pi^0$  ( $\pi^+\pi^-\eta$ ) invariant mass spectrum at the  $\eta$  ( $\eta'$ ) mass must be due to non-ISR processes, and this one is expected to dominate. From about 20 and 45 observed events, we derive cross sections for  $e^+e^- \rightarrow \eta\gamma$  and  $e^+e^- \rightarrow \eta'\gamma$  of  $4.5 \pm 1.2 \pm 0.3$  and  $5.4 \pm 0.8 \pm 0.3 \text{ fb}$ , respectively, where the first errors are statistical and the second systematic.

#### 3.2. Spacelike TFFs

We have measured the cross sections for the ‘two-photon’ processes  $e^+e^- \rightarrow e^+e^-\gamma^*\gamma^* \rightarrow e^+e^-X$ , for the pseudoscalar mesons  $X = \pi^0$  [12],  $\eta$  and  $\eta'$  [13] and  $\eta_c$  [14]. Here, both the electron and positron emit a virtual photon, the two photons interact to produce the meson  $X$ , and the  $e^+$  and  $e^-$  remain in the final state. We consider the ‘single tag’ case, in which one photon is nearly real ( $q_1^2 \approx 0$ ) and the  $e^+$  or  $e^-$  that emitted it travels along the beam line, and the other photon has  $Q^2 = -q_2^2 > 3 \text{ GeV}^2$  so that the  $e^-$  or  $e^+$  is within the detector acceptance. These cross sections can be related to the TFFs  $F_X(Q^2)$ .

The event selection is similar to that for ISR or timelike TFF measurements, but with an energetic  $e^\pm$  in place of the high-energy photon. Since the  $e^\pm$  is charged, we trigger on purely neutral recoil systems efficiently and reconstruct them well. We select events with a well identified  $e^\pm$  recoiling against a  $\gamma\gamma$  pair or a  $\pi^+\pi^-\pi^0$ ,  $\pi^+\pi^-\eta$  or  $K_S^0 K^+ \pi^-$  system, all well contained within the detector acceptance. To obtain clean samples of two-photon events with well measured  $Q^2$ , we make requirements on the 4-momenta of the detected  $e^\pm X$  systems, the missing 4-momenta, and the direction (forward or backward) of the detected  $e^\pm$ . We fit the invariant mass distributions of the recoiling systems to obtain the numbers of  $X$ -mesons in each bin of  $Q^2$ . We cover the  $Q^2$  range from 4  $\text{GeV}^2$ , below which the efficiency is low and changing rapidly, to 40 or 50  $\text{GeV}^2$ , above which no significant signal is seen.

These fits eliminate non- $X$  backgrounds. We estimate the backgrounds from  $e^+e^- \rightarrow q\bar{q}$  events using events with the  $e^\pm$  travelling in the wrong direction, and subtract them; they are very small. We estimate the backgrounds from other two-photon processes by reconstructing additional  $\pi^0$  candidates in the events, and by studying the shapes of the kinematic distributions used in the selection for data and simulated signal-like and background-like events. These backgrounds are also very small, but must be subtracted carefully. We observe a total of about 14,000  $e^+e^- \rightarrow e^+e^-\pi^0$  events, 2,800  $\eta$  events, 5,000  $\eta'$  events and 530  $\eta_c$  events.

#### 3.3. Results

For the  $\eta_c$  we also measure the cross section for untagged events, in which neither the  $e^+$  nor the  $e^-$  is detected, and which corresponds to  $F(0)$ . We use this for normalization, and the resulting  $F_{\eta_c}(Q^2)/F_{\eta_c}(0)$  is shown in Fig. 4(left) as a function of  $Q^2$ . It shows the expected falling behavior with  $Q^2$ , and the data points lie systematically below the leading order QCD prediction (dashed red line), indicating the need for a higher-order calculation. A fit to a monopole function,  $F(Q^2) = F(0)/(1 + Q^2/\Lambda)$ , gives a good  $\chi^2$  (blue line) and yields a parameter value of  $\Lambda = 8.5 \pm 0.6 \pm 0.7 \text{ GeV}^2/c^4$ , which is consistent with a prediction based on vector dominance of  $\Lambda = m_{J/\psi}^2 = 9.6 \text{ GeV}^2/c^4$ .

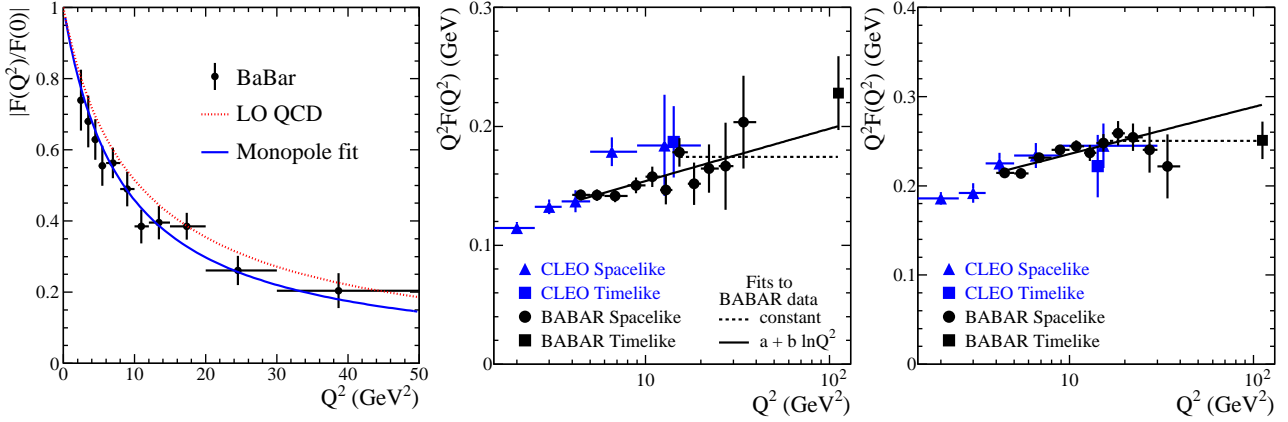


Figure 4: Left: transition form factor for the  $\eta_c$  meson as a function of  $Q^2$ , normalized to its value at  $Q^2=0$ . The dashed line represents the prediction of leading order QCD, and the blue line the result of the fit to the monopole function described in the text. Timelike (squares) and spacelike (circles) TFFs for the  $\eta$  (middle) and  $\eta'$  (right) mesons scaled by  $Q^2$ , along with previous results from CLEO (blue). The dotted and solid lines are constant and logarithmic fits, respectively, to the BaBar data for  $Q^2$  above 12 and 3  $\text{GeV}^2$ .

For the other mesons we convert our measured cross sections into TFFs and scale by  $Q^2$ , since the quantity  $Q^2 F_X(Q^2)$  is expected to approach an asymptotic value of  $\sqrt{2}f_X$ , where  $f_X$  is the  $X$ -meson decay constant. There are overall systematic uncertainties of 2.3%, 2.6% and 3.3% on the  $\pi^0$ ,  $\eta$  and  $\eta'$  data, respectively. The resulting  $Q^2 F_\eta(Q^2)$  and  $Q^2 F_{\eta'}(Q^2)$  are shown in the middle and right plots of Fig. 4, respectively, along with previous results from CLEO. The squares indicate timelike measurements and the circles spacelike TFFs. The CLEO and BaBar data are consistent, as are the timelike and spacelike results.

Both plots show the expected logarithmic rise with  $Q^2$  at low  $Q^2$ ; at higher  $Q^2$ , the data are consistent with both a continued rise and an approach to a constant value above about 10  $\text{GeV}^2$ . More precise and/or higher  $Q^2$  data are needed to determine the asymptotic behavior. Unfortunately, the values of  $f_\eta$  and  $f_{\eta'}$  are not well known, as they depend strongly on the degree of mixing between the two mesons. The predicted asymptotic values of  $Q^2 F(Q^2)$  span wide ranges that include both the highest- $Q^2$  data points and the values from the two fits at that  $Q^2$ .

The measured  $Q^2 F_\pi(Q^2)$  is shown in Fig. 5. It also shows the expected rise at low  $Q^2$  and is consistent with both a continued rise and a levelling off at higher  $Q^2$ . However, in this case there is a firm expected asymptotic value of  $\sqrt{2}f_\pi = 0.185 \text{ GeV}$ , shown by the dashed line, and the data are above this value for  $Q^2$  greater than about 10  $\text{GeV}^2$ . This indicates that the asymptotic value will be approached from above at much higher  $Q^2$  than is covered by the current measurements, if it is approached at all, and puts strong constraints on models for the distribution amplitudes.

At the time of this measurement, there were few theoretical predictions for the distribution amplitudes, and we tested them using the formalism of Bakulev, Mikhailov and Stefanis (BMS) [15]. The asymptotic form (ASY, see e.g. [17]) gives the magenta curve on Fig. 5; it lies systematically below the data and shows a slow approach to the asymptotic value from below. The amplitude of BMS [16] yields the green band on Fig. 5; it is similar in shape to the ASY prediction but higher everywhere and consistent with the data for  $Q^2$  below 8  $\text{GeV}^2$ ; however, it is inconsistent with the high- $Q^2$  data. The amplitude of Chernyak and Zhitnitsky CZ [18] yields the cyan line on Fig. 5; it is also similar in shape, but goes above the asymptotic line; it is consistent with the data for low and high  $Q^2$ , but inconsistent in shape and in the 4–14  $\text{GeV}^2$  region. We also fitted the function  $Q^2 F(Q^2) = A(Q^2/10 \text{ GeV}^2)^\beta$  to our data, obtaining parameter values of  $A = 0.182 \pm 0.002 \text{ GeV}$  and  $\beta = 0.25 \pm 0.02$ . The latter differs significantly from the value of 0.5 predicted by leading order QCD.

The  $\eta$  and  $\eta'$  states can be described as mixtures of strange ( $|s\rangle = |s\bar{s}\rangle$ ) and nonstrange ( $|n\rangle = (|u\bar{u}\rangle + |d\bar{d}\rangle)/\sqrt{2}$ ) states. One might expect the nonstrange state to have the same decay constant as the  $\pi^0$ ,  $f_n = f_\pi$  and an asymptotic TFF value of  $5\sqrt{2}f_n/3$ , with the factor of  $5/3$  due to quark charges. Similarly, for the strange component one might expect  $f_s = \sqrt{2f_K^2 - f_\pi^2} = 1.36f_\pi$  and an asymptotic TFF value of  $2f_s/3$ .

The mixing angle is not well known, but the properties of the nonstrange component are not very sensitive to the choice of angle. Using a mixing angle of  $41^\circ$ , we obtain  $F_n$  and  $F_s$  values from our data and the CLEO data. The quantity  $(3/5)Q^2 F_n(Q^2)$  is shown in Fig. 6(left), along with the BaBar  $Q^2 F_\pi(Q^2)$  data. It shows the expected general behavior, is consistent with approaching the expected asymptotic value from below, and is

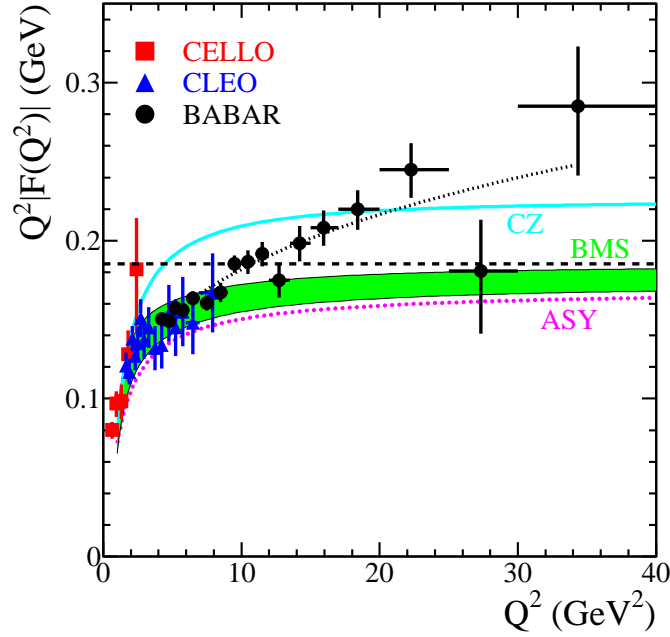


Figure 5: TFFs for the  $\pi^0$  meson scaled by  $Q^2$ , along with previous results from CLEO (blue) and CELLO (red). The dashed line indicates the expected asymptotic value of 0.185 GeV, and the dotted black line the result of a simple fit to a power of  $Q$  (see text). The green band and the cyan and magenta lines represent the theoretical predictions discussed in the text.

described very well by the BSM prediction. The  $Q^2$  dependence is also described by the ASY and CZ predictions. However, the scaled values are inconsistent with  $F_\pi$  for  $Q^2$  above 10  $\text{GeV}^2$ . The strange component is shown in the right-hand plot of Fig. 6. It shows similar general behavior, and the data points lie below a simple expectation of  $(\sqrt{2}/3)(f_s/f_\pi)$  times the ASY prediction from Fig. 5. However, the overall scale is sensitive to the mixing angle, as well as any other state mixing with the  $\eta'$ , so no conclusions can be drawn.

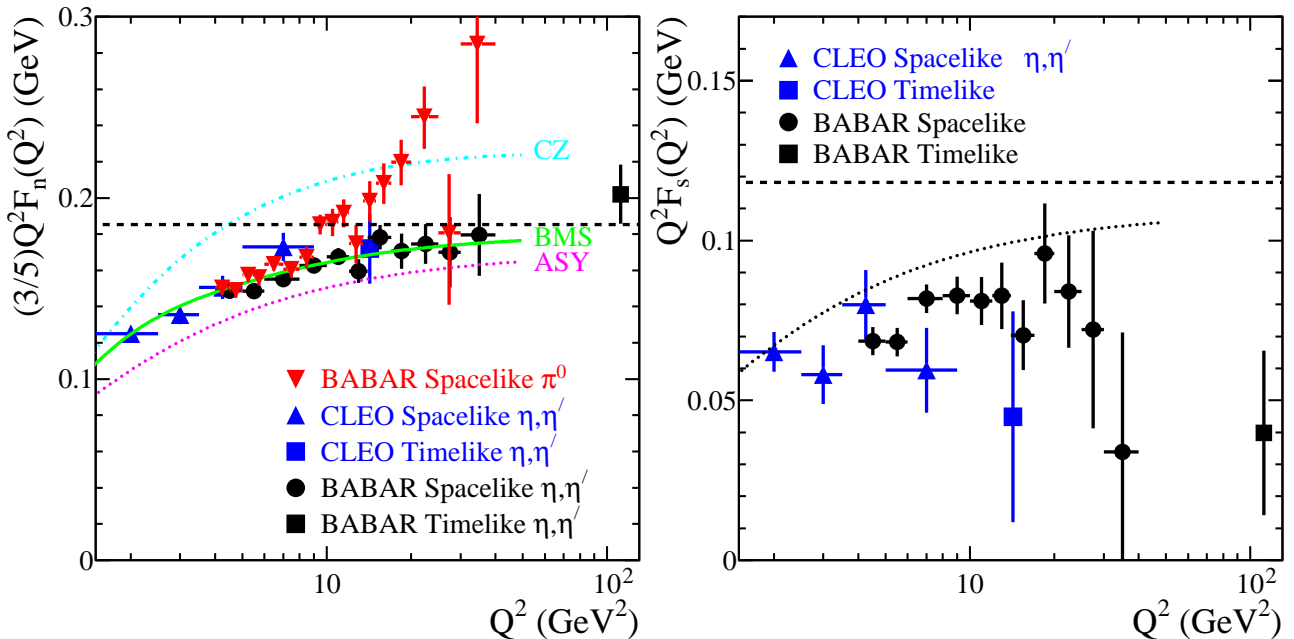


Figure 6: The nonstrange (left) and strange (right) TFFs extracted from the  $\eta$  and  $\eta'$  data using a mixing angle of  $41^\circ$ . The nonstrange data have been scaled by three-fifths for comparison with the  $\pi^0$  data and the theoretical predictions.

## 4. Summary

A very wide range of physics has been made possible by the high luminosity of the  $B$  factories, combined with state of the art detectors. In the area of hadronic spectroscopy, a large number of new states has been discovered or observed, including expected bottomonium and charmonium states, unexpected charmonium-like states, charmed mesons and baryons, the  $Y(2175)$ , and new  $\rho$  states. At Babar, we have studied the production of a number of hadronic final states via initial state radiation and two-photon interactions, which has provided a large body of information on lighter states, such as  $\eta$ ,  $\rho$ ,  $\omega$  and  $\phi$ , as well as the production characteristics of other light mesons and decay branching fractions of the  $J/\psi$  and  $\psi(2S)$  mesons.

Here we report improved measurements of the  $e^+e^- \rightarrow K^+K^-\pi^+\pi^-$  and  $e^+e^- \rightarrow K^+K^-\pi^0\pi^0$  cross sections, including a breakdown into resonant components. In particular, we obtain much improved values for the mass, width and production properties of the  $Y(2175)$  meson. However, its quark content and quantum numbers remain unknown. We also report a very precise measurement of the  $e^+e^- \rightarrow \pi^+\pi^-$  cross section at low energies that extends the range of such measurements greatly and will provide a good understanding of excited  $\rho$  states. It also improves our knowledge of the total hadronic cross section, which is vital for the interpretation of measurements of the muon anomalous magnetic moment,

We also summarize here our measurements of transition form factors for the pseudoscalar mesons  $\pi^0$ ,  $\eta$ ,  $\eta'$  and  $\eta_c$ . These are consistent with previous measurements at low  $Q^2$  and extend the  $Q^2$  range considerably. The measured TFFs for the three  $\eta$  states are consistent with expectations, although higher order QCD calculations are now needed. However, the TFF measured for the  $\pi^0$  is quite different from both the  $\eta$  mesons and the theoretical expectations at high  $Q^2$ . We look forward to renewed theoretical activity on this front.

## References

- 1 BaBar Collaboration, B. Aubert, et al., Phys. Rev. **D74**, 091103 (2006).
- 2 BaBar Collaboration, B. Aubert, et al., arXiv:1103.3001, submitted to Physical Review **D**.
- 3 DM1 Collaboration, A. Cordier, et al., Phys. Lett. **B110**, 335 (1982).
- 4 BES Collaboration, M. Ablikim, et al., Phys. Rev. Lett. **100**, 102003 (2008).
- 5 Belle Collaboration, C.P. Shen, et al., Phys. Rev. **D80**, 031101 (2009).
- 6 BaBar Collaboration, B. Aubert, et al., Phys. Rev. Lett. **103**, 231801 (2009).
- 7 CMD-2 Collaboration, V.M. Aulchenko, et al., JETP Lett. **82**, 743 (2005); JETP Lett. **84**, 413 (2006); R.R. Akhmetshin, et al., Phys. Lett. **B648**, 28 (2007).
- 8 KLOE Collaboration, F. Ambrosino, et al., Phys. Lett. **B670**, 285 (2009).
- 9 SND Collaboration, M.N. Achasov, et al., JETP Lett. **103**, 380 (2006).
- 10 M. Davier, et al., Eur. Phys. J. **C 71**, 1515 (2011).
- 11 BaBar Collaboration, B. Aubert, et al., Phys. Rev. **D74**, 012002 (2006).
- 12 BaBar Collaboration, B. Aubert, et al., Phys. Rev. **D80**, 052002 (2009).
- 13 BaBar Collaboration, B. Aubert, et al., Phys. Rev. **D84**, 052001 (2011).
- 14 BaBar Collaboration, B. Aubert, et al., Phys. Rev. **D81**, 052010 (2010).
- 15 A.P. Bakulev, S.V. Mikhailov and N.G. Stefanis, Phys. Lett. **B578**, 91 (2004).
- 16 A.P. Bakulev, S.V. Mikhailov and N.G. Stefanis, Phys. Lett. **B508**, 279 (2001) [Erratum-ibid **B590**, 309 (2004)].
- 17 S.J. Brodsky, and G.P. LePage, Phys. Lett. **B87**, 359 (1979).
- 18 V.L. Chernyak, and A.R. Zhitnitsky, Nucl. Phys. **B201**, 492 (1982) [Erratum-ibid **B214**, 547 (1983)].